Reactive Power Injection Capability of Buck–Boost Inverter With Unfolding Circuit

Carlos Roncero-Clemente, *Member, IEEE*, Oleksandr Husev, *Senior Member, IEEE*, Oleksandr Matiushkin, *Student Member, IEEE*, Dmitri Vinnikov, *Senior Member, IEEE*, and Frede Blaabjerg, *Fellow, IEEE*

***Abstract*—New emerging power inverter topologies are aiming at high-power density and efficiency with reliable performance. The recently proposed family of single-phase single-stage buck–boost inverters with output unfolding circuits have promising features for application in different fields. Nevertheless, the incapacity of injecting reactive power by the classical unfolding inverters has been assumed as its main drawback. Thus, our focus is on the reactive power injection capability of the single-stage buck–boost inverters with unfolding circuits. This attribute enables the converter to provide some extra ancillary services for friendly integration of the renewable energy resources and energy storage systems, providing support to the smart grid/microgrid, thus contributing to its power quality welfare. By means of a comprehensive analysis and implementation of proper closed-loop model predictive control, together with an adequate selection of the output capacitor, the single-inductor unfolding buck–boost inverter is capable of delivering reactive power to the utility grid. We used the simulation and experimental tests to validate the theoretical aspects.**

***Index Terms*—Ancillary services, buck–boost inverter, reactive power injection, single-stage inverter, unfolding circuit.**

I. Introduction

FOR a long time, grid-connected inverters for renewable energy resources (RESs) have sought to perform at the unity power factor [1], [2]. Nevertheless, as the electric systems and the trends toward the smart grid concept are spreading, any utility should be able to provide ancillary services to satisfy grid power requirements [3]. One of these main grid services is the reactive power interchange for voltage support [4].

Concurrently, many inverter topologies have been proposed for small-scale RESs aiming at high-power density, efficiency, and reliability [5]–[13]. For instance, the solutions based on dual-back inverters do not permit a wide range of voltage operations [5], [6] although this feature is mandatory on that power level and application field with the renewables. Neither does the differential boost inverter composed of two boost dc-dc branches allow for a wider voltage regulation despite counting with multiple inductors [7]. Another topology developed is based on the Ćuk-derived buck–boost inverter [8], [9]. In this solution, the drawback lies in the higher current spikes in the power elements. A single-stage inverter based on impedance-source networks has attracted increased research interest during the last years [10]–[12] because of advantages such as buck–boost functionality and shoot-through immunity. Nevertheless, some papers highlight the problems in terms of power density, efficiency, and complexity [13]. For those reasons, this family has not succeeded in industrial applications.

Unfolding bridge-based topologies are of high universal value in small inverters because of their high efficiency. However, initial solutions based on this approach do not allow for reactive power delivery, and slight zero-crossing current distortion also appears. These limitations are due to the presence of a diode between the first and the second power stage and the thyristors used in the unfolding bridge [14]–[19]. According to the dc-link stage, the different unfolding circuit-based inverters can be divided into three classes:

a) with a dc-link [14], [15];
b) with a pseudo dc-link [16], [17]; or
c) without a dc-link stage [18], [19].

Some studies have demonstrated the possibility of injecting reactive power with the unfolding inverter bridge by means of novel control schemes [20]. In that case, the zero-crossing current points keep the same position with the zero-crossing voltage, at the same time, distorting the current shape and deriving a worse power quality. Besides, some finalists of the Little Box Challenge proposed topological solutions based on advanced unfolder inverter circuits [21], [22]. These papers do not provide sufficient details for the analysis of reactive power injection. Furthermore, the unfolding circuit was controlled at a high switching frequency with a pulsewith modulation (PWM) operation if the load voltage is below a minimum value to avoid

Manuscript received January 20, 2022; revised April 13, 2022; accepted May 30, 2022. Date of publication June 2, 2022; date of current version June 24, 2022. This work was supported by the Estonian Research Council under Grant PRG675, in part by the Estonian Centre of Excellence in Zero Energy and Resource Efficient Smart Buildings and Districts (ZEBE), in part by the Junta de Extremadura (Regional Government) within the program "Ayudas Talento" (TA18003), the regional project (IB20165), and in part by the "Fondo Europeo de Desarrollo Regional (FEDER)." Recommended for publication by Associate Editor K. Basu. *(Corresponding author: Carlos Roncero-Clemente.)*

Carlos Roncero-Clemente is with the Department of Electrical, Electronic and Control Engineering, University of Extremadura, 06006 Badajoz, Spain (e-mail: carlosrc@unex.es).

Oleksandr Husev and Dmitri Vinnikov are with the TalTech University, 12616 Tallinn, Estonia (e-mail: oleksandr.husev@taltech.ee; dmitri.vinnikov@taltech.ee).

Oleksandr Matiushkin is with the TalTech University, 12616 Tallinn, Estonia, and also with the Chernihiv Polytechnic National University, 14000 Chernihiv, Ukraine (e-mail: oleksandr.matiushkin@taltech.ee).

Frede Blaabjerg is with the Aalborg Universitet, 9220 Aalborg, Denmark (e-mail: fbl@energy.aau.dk).

Color versions of one or more figures in this article are available at https://doi.org/10.1109/TPEL.2022.3179784.

Digital Object Identifier 10.1109/TPEL.2022.3179784

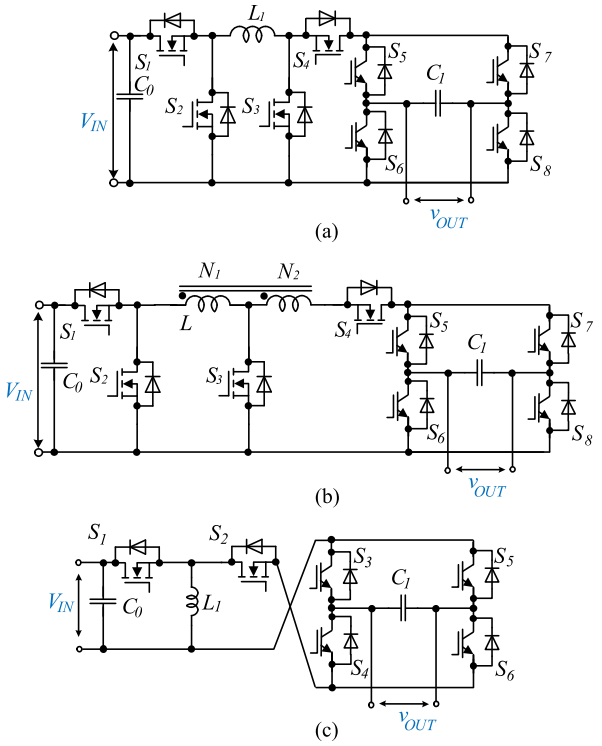

Fig. 1. Family of the single-phase single-stage buck–boost inverters with unfolding circuits proposed in [24]. (a) Single-inductor unfolding buck–boost inverter. (b) Tapped inductor unfolding buck–boost inverter. (c) Single-inductor twisted unfolding buck–boost inverter.

the zero-crossing current distortion. Finally, the discussion of the filter capacitor is essential when the system operates at a power factor different from one [23].

Subsequently, the new family of single-stage buck–boost inverters with an unfolding circuit recently proposed in [24]–[26] (see Fig. 1) are innovative, with some modifications introduced in their former counterpart. This new family allows for full bidirectionality of power, and the capacitor is placed at the ac side, which permits power decoupling at a smaller size. At the same time, this family of converters has in fact a pseudo dc link, thus the reactive power delivery is possible with an appropriate control scheme [23]. Nevertheless, some recent studies still consider such solutions as unity power factor inverters [27], [28]. Finally, derived solutions proposed in [29] are HERIC-based with active clampling, having bidirectional power flow, but they demonstrated just the unity power factor testing and results.

In this framework, the motivation of this article is to demonstrate the reactive power injection capability of the single-stage buck–boost inverters with an unfolding circuit, making it capable of providing voltage grid support, for example, during a voltage sag (so-called low-voltage ride-through functionality). Section II explains the reactive power injection principle and the main operation modes with their equivalent circuits when delivering reactive power leading and lagging. The study and these equivalent circuits are intended specifically for the single-inductor unfolding buck–boost inverter topology [see Fig. 1(a)]. Besides, considerations for the design of the output capacitor C_1 are given there. Then, a general control scheme with the funding based on the model predictive control (MPC) [30]

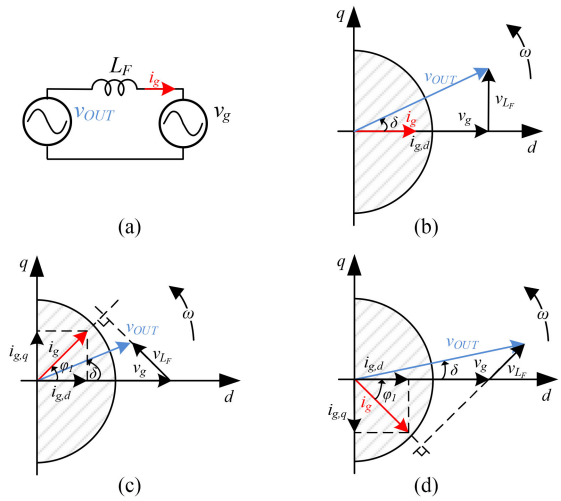

Fig. 2. Simplified equivalent circuits and phasor diagrams of the system: (a) simplified circuit, (b) active power injection, (c) active and capacitive reactive power injection, and (d) active and inductive power injection.

implemented is described in Section III. Sections IV and V show the simulation and the experimental results, respectively. Finally, conclusions are presented in Section VI.

II. Reactive Power Injection Capability and Operation Analysis

This section describes the operation principle during the reactive power injection with the single-inductor unfolding buck–boost inverter [see Fig. 1(a)]. Different operation modes with their equivalent circuits are explained as well.

A. Basic Principle

A simplified equivalent circuit at the line frequency in Fig. 2(a) represents any of the inverter circuits from Fig. 1 connected to the main grid via an L filter (L_f); the complex power delivered from one node to another is given by $\vec{S}_G = \vec{V}_g \vec{I}_g^*$. $\vec{V}_g$ and $\vec{I}_g^*$ represent the grid voltage phasor and the grid current conjugate complex, respectively. By splitting the equation into the real and imaginary parts, the expression for the delivered active (P_G) and the reactive power (Q_G) is

$$P_G = \frac{V_{\mathrm{OUT}} V_g \sin\delta}{X_{\mathrm{LF}}}\ ,\ Q_G = \frac{V_g\left(V_{\mathrm{OUT}}\cos\delta - V_g\right)}{X_{\mathrm{LF}}}\ . \qquad (1)$$

In (1), V_{OUT} and V_g correspond to the rms voltage values of the output capacitor C_1 and the grid voltages, δ is their phase shift, and X_{LF} is the reactance of L_f. Thus, by means of regulating both δ and V_{OUT} of the inverter, the active and the reactive power flows can be controlled. At the same time, the instantaneous current and voltages in Fig. 2(a) can be transformed into their *dq* magnitudes. Three cases depending on the grid current phasor are also presented by the phasor diagrams in Fig. 2 on the rotating reference frame. The grid voltage is adopted as a reference, so it just contains a direct component *d*. In Fig. 2(b), only the direct component of the grid current ($i_{g,d}$) is delivered to the main grid. The inductive filter implies a small difference between the C_1 output capacitor voltage and the grid voltage, both in the phase shift and in the amplitude. Fig. 2(c) and (d) shows the

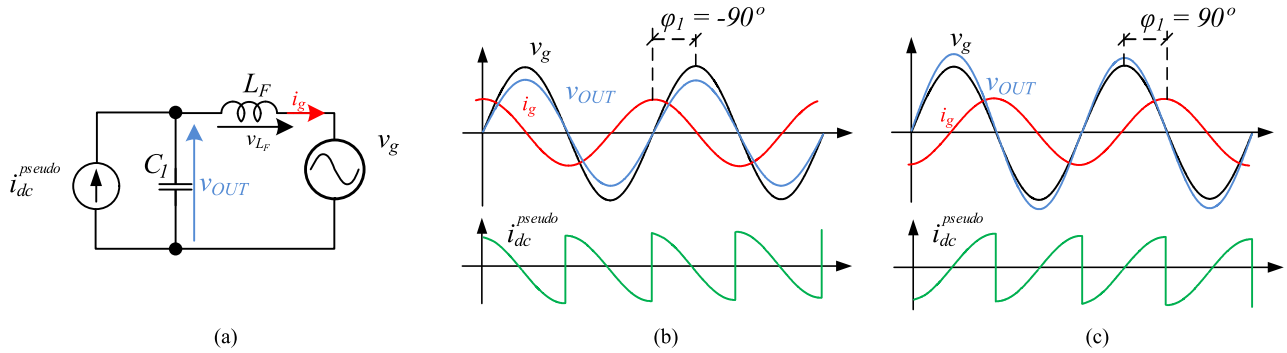

Fig. 3. Illustration of the reactive power injection operation: (a) equivalent circuit with a controlled current source representing the pseudo dc link, (b) idealized waveforms when $\varphi_1 = 90$ (pure capacitive reactive power injection), and (c) idealized waveforms when $\varphi_1 = -90$ (pure inductive reactive power injection).

phasor diagram when the q component of the grid current ($i_{g,q}$) is positive and negative (capacitive and inductive reactive power injection), respectively. In these situations, the grid current has a q component with a positive sign [see Fig. 2(c)], producing a decreased capacitor amplitude voltage compared to the grid amplitude voltage. In Fig. 2(d), the q component is negative and the capacitor voltage increases compared to the grid voltage. In Fig. 2, φ_1 is the phase shift between the instantaneous output current (i_g) and the instantaneous grid voltage (v_g), and v_{LF} is the voltage drop in the output filter.

B. Operation Modes

According to the classification proposed in [31], the single-phase single-stage buck–boost inverter family object of this work belongs to the topologies that include a pseudo dc link. The single-inductor unfolding buck–boost inverter [see Fig. 1(a)] has a modulated dc–dc converter at the initial stage that produces a rectified sinusoidal voltage in the pseudo dc link. The line-frequency commutated circuit unfolds the pseudo dc-link voltage to the sinusoidal shape at v_{OUT}, being capable of fully operating in a bidirectional way with the power switches $S_1, \ldots, S_4$. Thus, one of the main purposes is to generate the unfolding circuit switching synchronized with v_g.

In the equivalent circuit presented in Fig. 3(a), the modulated dc-dc converter is replaced by a fully controllable current source ($i_{\mathrm{dc}}^{\mathrm{pseudo}}$) connected to the main grid. The unfolder dynamics are ignored as the switching frequency of $S_1, \ldots, S_4$ is much higher than the line frequency. Furthermore, Fig. 3(b) and c illustrates the idealized shapes of the main signals v_{OUT}, v_g, i_g, and $i_{\mathrm{dc}}^{\mathrm{pseudo}}$ when the converter is delivering pure capacitive ($\varphi_1 = 90°$) and inductive ($\varphi_1 = -90°$) reactive power, respectively, representing the limit cases, where δ is equal to zero. Note that the amplitude of v_{OUT} is decreased and increased compared to v_g, respectively, as shown in the corresponding phasor diagrams in Fig. 2. At the same time, $i_{\mathrm{dc}}^{\mathrm{pseudo}}$ will have the same shape as i_g during the positive half cycle of v_{OUT} (from 0° to 180°), and the negative shape of i_g during the negative half cycle of v_{OUT} (from 180° to 360), as expected.

For the particular case presented in Fig. 3(b), where the converter is delivering leading reactive power, three different operation modes for the single-inductor unfolding buck–boost inverter are distinguished, detailed, and discussed in Fig. 4(a)–(c). In Fig. 4(a), the situation corresponds to positive values of v_{OUT} and i_g. The main switches S_7 and S_6 of the unfolding inverter are ON, whereas the switches S_5 and S_8 are OFF. At the same time, the pairs S_1-S_2 and S_3-S_4 [see Fig. 1(a)] are complementarily switching at high frequency. In the situation depicted in Fig. 4(a) in $t = t_0$ and in $t = t_1$, i_g is positive thus the operation is forward. In $t = t_0$, the current error (Δi) is positive, thus S_1 and S_3 are ON order to charge L_1 from the input source. Note that the MPC has calculated the optimal duty cycle (D_t) based on several criteria [30]. During the complementary state ($t = t_1$), S_1 is OFF and the stored energy in L_1 is transmitted to the output through the wheeling diode of S_4. Nevertheless, in Fig. 4(b) in $t = t_0$ and in $t = t_1$, i_g is negative thus the operation is reverse. In $t = t_0$, Δi of $i_{\mathrm{dc}}^{\mathrm{pseudo}}$ is positive (note that $i_{\mathrm{dc}}^{\mathrm{pseudo}}$ is negative), thus S_2 and S_4 are ON to charge L_1 from the output side. In this case, $i_{\mathrm{dc}}^{\mathrm{pseudo}}$ will increase its value, but remain negative. In the complementary state, when Δi is negative and $t = t_1$, S_1 and S_3 are conducting and $i_{\mathrm{dc}}^{\mathrm{pseudo}}$ charges C_0, decreasing its value again. Finally, in Fig. 4(c), i_g is still negative thus the operation remains reverse. However, in this case, $i_{\mathrm{dc}}^{\mathrm{pseudo}}$ is positive as in the case presented in Fig. 4(a), thus the control switching strategy is the same as in there, with the only difference that the unfolding bridge has opposite polarity compared to Fig. 4(a). At the same time, the unfolding circuit reverses the state and switches S_5 and S_8 are conducting; meanwhile, switches S_7 and S_6 are OFF. $i_{\mathrm{dc}}^{\mathrm{pseudo}}$ has to change the current polarity to the opposite. To provide this current jump, switches S_1 and S_3 are ON until reaching the required value of the current (note that this switching state provides the maximum positive current slope), being this switching state, the most dominant during the sign current change, where the inductance L_1 is short-circuited with the input voltage source. A detailed description of the operation modes is available [32].

Finally, the presence of a small capacitor C_2 (with a value equal to 100 nF) placed before the unfolding circuit is marked in Fig. 4(a)–(c). C_2 allows the inductor current flowing into it when the unfolding stage is switched OFF. This operation state appears if φ_1 is equal to $-90°$, where $i_{\mathrm{dc}}^{\mathrm{pseudo}}$ has a positive value during the unfolding stage switching.

It should be mentioned that the presented equivalent circuits and the idealized waveforms assume a small value of the

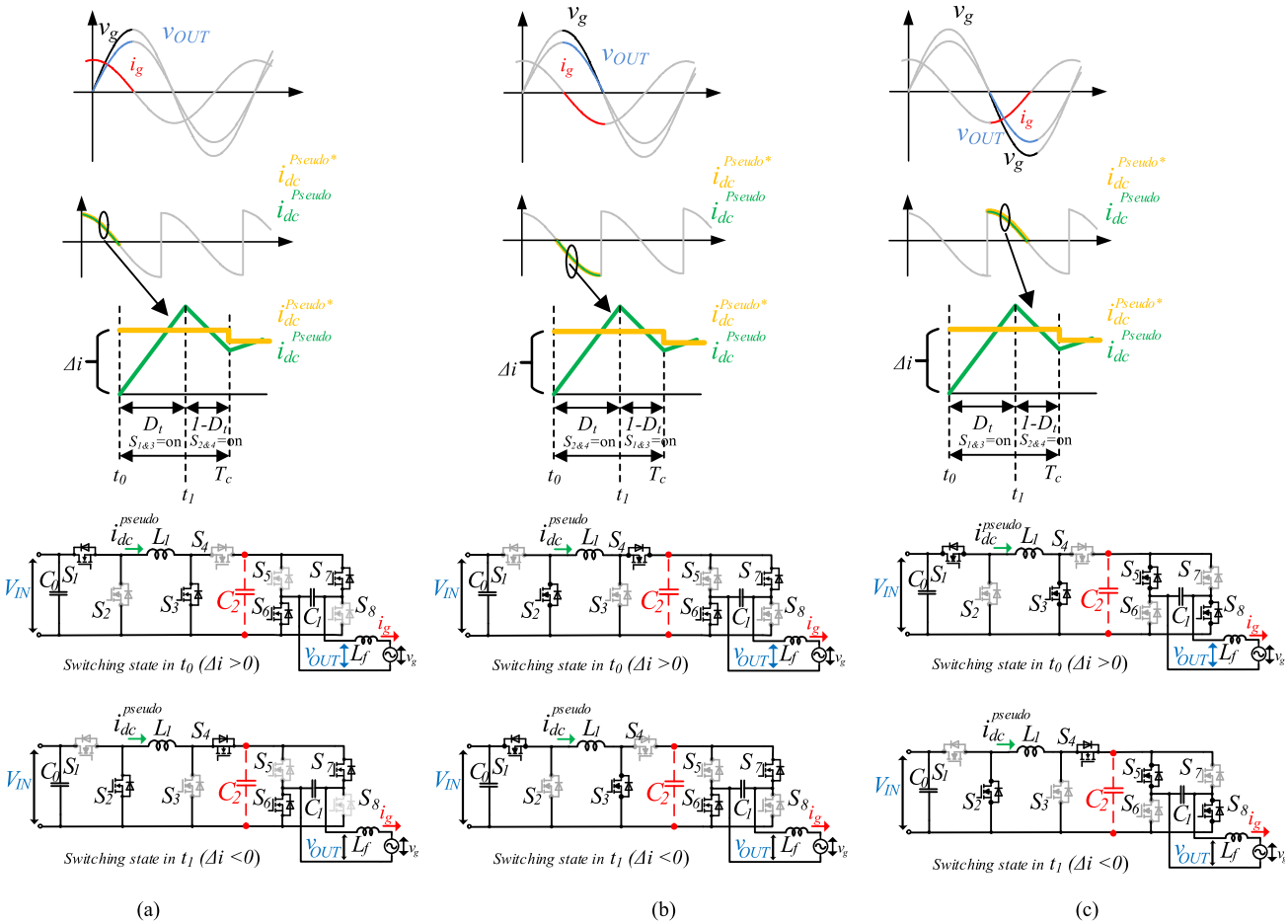

Fig. 4. Operation modes of the single-inductor unfolding buck–boost inverter injecting pure capacitive reactive power: (a) v_{OUT} and i_g are both positive, (b) v_{OUT} is positive and i_g negative, and (c) v_{OUT} and i_g are both negative.

capacitor C_1 to filter the high switching frequency current ripple. As the capacitor C_1 value increases, the current step or jump in L_1 in the case of Fig. 4(c) is smoothened. Considerations about the C_1 value and its influence will be discussed in the following section.

C. Considerations for the Output Capacitor C_1 Value

Fig. 5 illustrates the most unfavorable situation. It corresponds to the negative phase shift between the grid current and voltage [see Fig. 5(a)]. The equivalent circuit before the voltage zero crossing is shown in Fig. 5(b). It can be seen that the current through the buck–boost inductance as well as output grid current have a positive direction. Straight after grid voltage zero crossing, the unfolding circuit reverses the switches and the inductor current will be directed opposite. The main problem is that the voltage across the capacitor is close to zero, and a very rapid buck–boost inductor current changing similar to the positive phase shift is not possible. It will lead to the grid current waveform distortion. To minimize this, the current across the buck–boost inductor has to be equal to zero at the moment of the unfolding circuit switching and the value of the capacitor has to be sufficiently large.

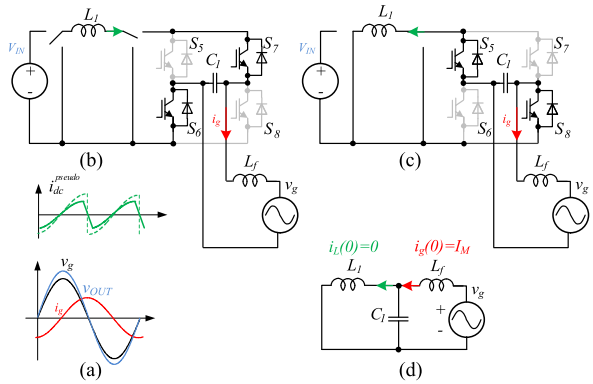

Fig. 5. Equivalent circuits and idealized waveforms during the unfolding switching and active and capacitive reactive power injection: (a) $i_{\mathrm{dc}}^{\mathrm{pseudo}}$, v_g, v_{OUT} and i_g, (b) equivalent circuit before the unfolding switching, (c) equivalent circuit after the unfolding switching, and (d) equivalent transient circuit.

The circuit straight after the unfolding switching is shown in Fig. 5(c). The equivalent circuit of this transient process is represented in Fig. 5(d). The main goal of this subsection is to find the capacitor value and the time interval of the equivalent circuit that provide the minimum grid current distortion.

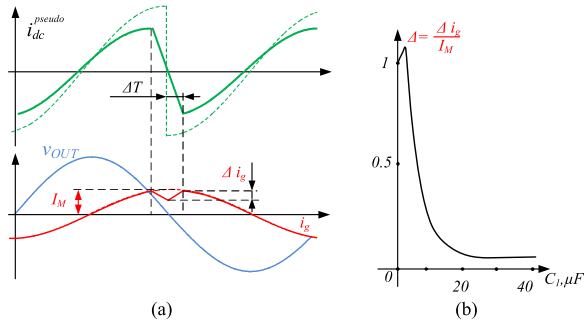

Fig. 6. Current dip during the unfolding circuit switching: (a) simplified voltage and current waveforms and (b) dip dependences as a function of capacitor value of C_1.

TABLE I
COMPONENTS CALCULATION FOR CURRENT DIP MITIGATION

Parameter	Value (Size)
Switching frequency	62.5 kHz
Sampling frequency	62.5 kHz
Loop bandwidth	6.25 kHz
Inductor L_1	1.6 mH
Grid side inductance L_f	330 µH
Grid current relative dip value	≤3%
Equivalent circuit (Fig. 5*c*) duration time $\Delta T=1/F_s$	16 µs
Maximum reactive grid current I_M	5 A

To define the required value of the unfolding capacitor, the set of differential equations is defined as follows:

$$\begin{cases} v_g = L_f \frac{di_g}{dt} + L_1 \frac{di_L}{dt} \\ v_g = L_f \frac{di_g}{dt} + v_{C1} \\ C_1 \frac{dv_{C1}}{dt} = i_g - i_L \end{cases} \tag{2}$$

where

$$v_g = V_M \sin(\omega t). \tag{3}$$

The solution of these equations for the grid current enables us to find the current dip that will be observed after the unfolding switching as a function of the capacitor value C_1. At the same time, the initial expression is very bulky. Analyzing the most important components, the value of the recommended capacitor can be expressed as follows:

$$\mathrm{C}_1 \geq \frac{L_1 + L_f}{L_1 \cdot L_f} \cdot \Delta T^2 \cdot \frac{1}{\arccos(1 - \Delta - \Delta \frac{L_f}{L_1})} \tag{4}$$

where Δ is the relative current dip at the moment of the unfolding circuit switching and ΔT is the duration time of the equivalent circuit in Fig. 5(c). The result is illustrated graphically in Fig. 6. It shows that with the capacitor increasing, the current ripple is decreasing. To simplify the final expression, it was also assumed that the grid voltage sinusoidal dependence can be replaced by linear dependence. Fig. 6 shows the current spike [see Fig. 6(a)] and its dependence on the capacitor value C_1.

Table I shows the example of the calculation results of the passive components taking into account that the minimal duration ΔT of the equivalent circuit depicted in Fig. 5(c) is equal to the sampling time of the system.

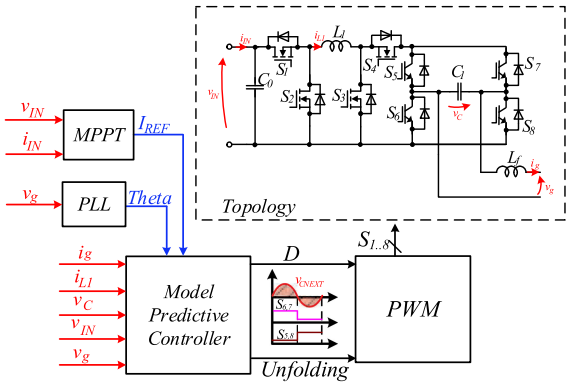

Fig. 7. Structure of the control system based on MPC.

III. CLOSED-LOOP MODEL PREDICTIVE CONTROL (MPC)

MPC is the control approach for the reactive power generation with the proposed system. The work presented in [30] describes the details of the selected controller. General statements of the MPC for the buck–boost inverter based on the unfolding circuit are discussed in this section. Fig. 7 shows the structure of the control system. The MPC is realized based on the continuous control set because of the use of the PWM. In a very general case, it may contain the maximum power point tracking algorithm for photovoltaic applications or any other algorithm that sets the reference value and can synchronize the converter with the grid side by the phase-lock loop. In our application, the main parameter that is needed to control is i_g, however, due to the particularity of the unfolding bridge and its switching, i_g will not be controlled with quality enough, thus we use a special cost function in our control system based on controlling the inductor current.

It is assumed that the buck–boost inverter is a nonminimum phase system that complicates the requirements for the control unit. That is why the cost function in this application observes the buck–boost inductor current:

$$J = \min \left\{ \sum_{j=1}^{2} \left(\begin{array}{l} |i'_{L1}[k+j] - i_{L1\mathrm{REF}}[k+j]| \cdot W_{j1} + \\ + |i_{L1}[k+j] - i_{L1\mathrm{REF}}[k+j]| \cdot W_{j2} \end{array} \right) \right\} \tag{5}$$

where $i'_{L1}[k+j]$, $i'_{L1}[k+1]$, $i'_{L1}[k+2]$, $i_{L1}[k+j]$: $i_{L1}[k+1]$, and $iL1[k+2]$ are predictive values of the inductor current during the next PWM periods, and $iLREF[k+j]$: $iLREF[k+1]$, and $iLREF[k+2]$ are reference values of the inductor current.

The MPC predicts the next two samples of the system that correspond to two horizons. However, the second horizon was clipped and was used with an approximation for faster computations. The overall number of cycle iterations is 10.

The amount of the duty cycle step is also reduced due to the limitation of the microcontroller. This approach increases reliability and allows us to decrease the time of computations. The system predicts the next duty cycle value across the previous value considering a 10% range

$$D[k+1] = D[k] \pm 0.1 \tag{6}$$

where $D[k]$ is the previous value of the duty cycle.

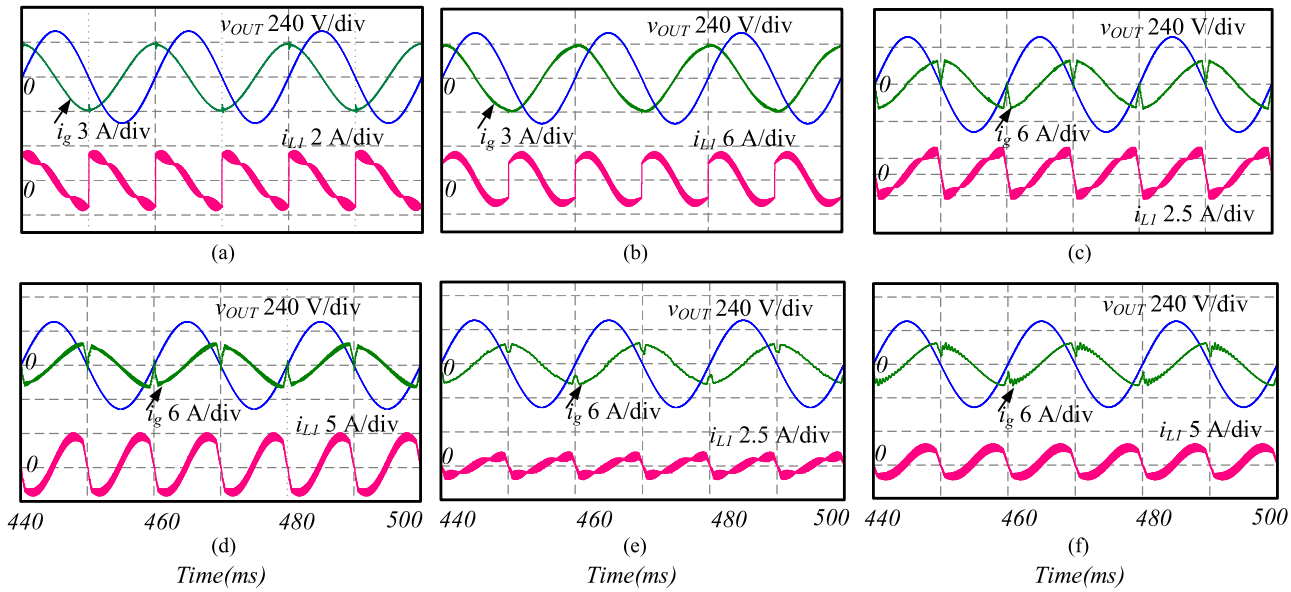

Fig. 8. Main simulation results with the selected waveforms $v_{\rm OUT}$, ig, and i_{L1}: (a) single-inductor inverter injecting pure inductive reactive power ($\varphi_1 = 90°$) and $C_1 = 1.3$ μF, (b) single-inductor twisted inverter injecting pure inductive reactive power ($\varphi_1 = 90°$) and $C_1 = 1.3$ μF, (c) single-inductor inverter injecting pure capacitive reactive power ($\varphi_1 = -90°$) and $C_1 = 1.3$ μF, (d) single-inductor twisted inverter injecting pure capacitive reactive power ($\varphi_1 = -90°$) and $C_1 = 1.3$ μF, (e) single-inductor inverter injecting pure capacitive reactive power ($\varphi_1 = -90°$) and $C_1 = 15$ μF, and (f) single-inductor twisted inverter injecting pure capacitive reactive power ($\varphi_1 = -90°$) and C_1=15 μF.

The heuristic methodology allowed us to find the optimal weighting factors *W*11, *W*12, *W*21, and *W*22. According to the second horizon, it should be with a higher priority; thus, the ratio between the second horizon weight factors and the first one is 2:1. The last important statement is that the grid current cannot change sharply. As a result, the grid current samples can be expressed as follows:

$$i_g\,[k+3] = i_g\,[k+2] = i_g\,[k+1] = i_g\,[k] \qquad (7)$$

where *ig[k*+3*], ig[k*+2*],* and *ig[k*+1] are predictive values of the grid current for the next PWM periods.

IV. Simulation Study

To verify the theoretical statements presented above, a comprehensive simulation study was performed in PSIM software. As one of the main application fields of the converter family under study is in the power conversion involving renewable energies, the input voltage $V_{\rm IN}$ was set at 250 V. The system is connected to a single-phase utility grid with nominal phase-to-neutral rms voltage equal to 230 V. In this situation, the power converter is forced to alternate the buck and the boost operation every fundamental cycle.

All the converters shown in Fig. 1 were tested in the simulation: the single-inductor unfolding buck–boost inverter, the tapped inductor unfolding buck–boost inverter, and the single-inductor twisted unfolding buck–boost inverter. As the tapped inductor unfolding buck–boost inverter showed the same results as the single-inductor unfolding buck–boost inverter, the former will not be discussed here.

At the same time, the buck–boost inductance L_1 was equal to 1.6 mH, and the unfolding capacitor C_1 was 1.3 μF. The grid filtering inductance L_f was equal to 0.33 mH, and the switching frequency ($f_{\rm sw}$) was 62.5 kHz. The MPC presented above was implemented and tuned to provide a good quality of the i_g and $i_{\rm dc}^{\rm pseudo}$. The current control loop bandwidth is $f_{\rm sw}$/10 [33].

Fig. 8(a)–(f) shows the most interesting waveforms of the simulation study for both the single-inductor unfolding buck–boost inverter and the single-inductor twisted unfolding buck–boost inverter. Instantaneous values of v_g, i_g, and inductance current (i_{L1}) are presented in the subfigures. In Fig. 8(a), the simulation results correspond to a buck–boost inverter with an unfolding circuit injecting just inductive reactive power with a small value of the unfolding capacitor C_1.

The reference reactive power for that case was 500 var. The same test was performed using the single-inductor twisted unfolding buck–boost inverter and the results are depicted in Fig. 8(b). In both cases, a good sinusoidal shape of the grid current is achievable.

The opposite phase shift in the reference current was programmed for both power converters as well. Thus, pure capacitive reactive power ($\varphi_1 = -90°$) is injected into the grid in Fig. 8(c) and (d) (the reference reactive power was -500 var). In this situation, some current spikes appear in i_g during the zero-crossing of the grid voltage. During the zero-crossing of the grid voltage, the current across the inductor has to change the flow direction from positive to negative at the same time as the unfolding inverter switch [similar to the transition between the equivalent circuits from Fig. 8(b) and (c)]. As the capacitor voltage $v_{\rm OUT}$ is very low, the current speed rate in the inductance is very high in this transition.

To mitigate the zero-crossing distortion of the i_g, the unfolding capacitor was increased from 1.3 to 15 μF. The obtained results for the single-inductor unfolding buck–boost inverter and the

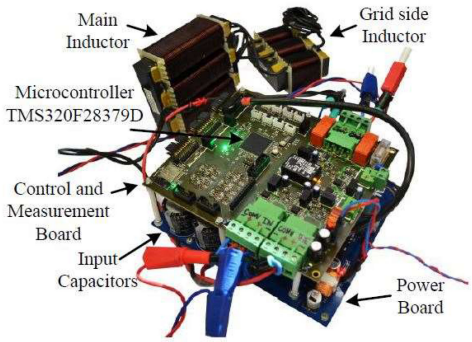

Fig. 9. Experimental prototype of the twisted unfolding buck–boost inverter.

TABLE II
PROTOTYPE SPECIFICATION

Parameter	Value
Grid voltage	115 V, RMS
Input voltage range	50 V - 250 V
Maximum input current I_{IN}	10 A
Maximum grid current I_g	16 A, RMS

single-inductor twisted unfolding buck–boost inverter are represented in Fig. 8(e) and (f), respectively. The figures show that the grid current has improved its quality significantly.

It is important to note that we analyzed the most extreme cases, i.e., pure inductive and capacitive power injection to the utility grid. By this approach, the unfolding inverter was controlled at the line frequency at any time. Thus, the full range of the power factor (lagging to leading) can be covered with high efficiency. Other control solutions as the unfolding circuit operation with a PWM near the zero-voltage [22] may limit the power factor range besides the reduction in the power converter efficiency.

V. EXPERIMENTAL VERIFICATION

To validate the reactive power injection capability of the single-phase single-stage buck–boost inverter with the unfolding circuit, a prototype of the twisted unfolding buck–boost inverter [see Fig. 1(c)] was designed, assembled, and tested (see Fig. 9). Table II shows the specification of the prototype.

The system for the experimental setup is divided into two main printed circuit boards (PCBs), one with the power hardware and the other for the control hardware. The passive components are the same as in the simulation study for a fair comparison. The power electronic switches of the prototype are composed of SiC Mosfet transistors C2M0080120D. The unfolding circuit is based on the Infineon Mosfet transistors IPB60R060P7ATMA1.

The control PCB contains the different sensors required for the closed-loop MPC control and the synchronization block. The current sensors ACS720 by Allegro allow a good overcurrent protection with their digital outputs. The measurement stage was isolated from the controller. The control unit is based on the TMS320F28379D microcontroller by Texas Instruments. Our experiments were conducted with a digital oscilloscope Tektronix MDO4034b-3, with current probes Tektronix TCP0150 and voltage probes Tektronix TPA-BNC.

The components were selected according to the methodology demonstrated in [25], [34]. The so-called power decoupling approach is widely used in the single-phase systems [35], [36] to mitigate the input current ripple. The simple input decoupling capacitors widely used in industry are applied in this case.

Fig. 10 shows the main obtained experimental results, and variables v_g, i_g, and inductance current (i_{L1}) selected. Several unfolding capacitors were used in experimental verification. Fig. 10(a) shows the case where the twisted unfolding buck–boost inverter is delivering 400 var, i.e., just inductive reactive power is injected into the grid with $\varphi_1 = 90°$. The inductor current shows a waveform similar to the ideal shape mentioned above. It can be seen that due to the high average value of the current, the high-frequency ripple is very small. Furthermore, the output current distortion during the zero-crossing of the grid voltage is negligible. In the second test, the pure capacitive reactive power injection to the grid ($\varphi_1 = -90°$) was verified. The reference reactive power was equal to -400 var. Similar power quality in the grid current was obtained, proving the same adequate performance [see Fig. 10(b)]. Finally, an intermediate case where the power inverter injects active power and inductive reactive power (330 W and 240 var) was studied, corresponding to a power factor equal to 0.8 ($0° < \varphi_1 < 90°$). The results of this test are shown in Fig. 10(c). i_g demonstrates very good quality.

Fig. 11 shows additional steady-state experimental results with the transient process. The unfolding capacitor was equal to 30 μF. Fig. 11(a)–(c) corresponds to the positive shifting on 90° of the grid current (measured THD of i_g was 4.64%). The current in inductance cannot change immediately. Thus, the inductor current cannot "jump" to a value with a different polarity, not even if 100% of the duty cycle is applied. In this particular case, it requires three PWM periods with 95% of the duty cycle for changing the inductor current from a negative to a positive value, as it is shown in Fig. 11(b) and (c). The voltage across the inductor follows the expected voltage value without any spikes. Moreover, the voltage across the inductor becomes negative during the operation mode presented in Fig. 4(b), during only the nonzero grid voltages.

Fig. 11(d)–(f) shows the operation with a negative phase shift between the grid current and the grid voltage (measured THD of i_g was 9.27%). The voltage across the inductor switches from the positive input source voltage value to the minus grid voltage value, as it is demonstrated in Fig. 11(f). In this sense, the inductor voltage is changing according to the steady-state analysis strategy.

Finally, Figs. 12 and 13 show the experimental results of the dynamic response. In the first case [see Fig. 12(a)–(c)], the grid current changes from 8 A of the active power to 2 A of the reactive power with a phase shift of 90° to the grid voltage. Fig. 12(b) indicates the shapes of the input current and voltage and the grid current and voltage during the current step. The inductor current and the unfolding capacitor voltage are shown in Fig. 13(c). The experimental results did not show abnormal shapes of the grid current during the current step. MPC allowed us to avoid any spikes during the transient process, going very fast to the new reference current value. The second case corresponds to a negative phase shift of $-90°$ of the grid current, with

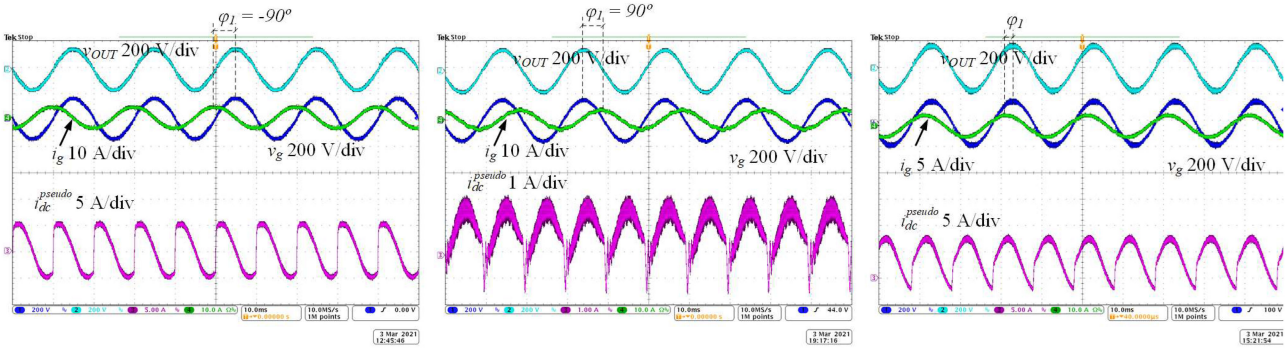

Fig. 10. Experimental results (v_{OUT}, i_g, and i_{L1}) with the twisted unfolding buck–boost inverter delivering reactive power to the grid: (a) pure inductive reactive power injection ($\varphi_1 = 90°$) and $C_1 = 15$ μF, (b) pure capacitive reactive power injection ($\varphi_1 = -90°$) and C_1=15 μF, and (c) active and inductive reactive power injection ($0° < \varphi_1 < 90°$) and $C_1 = 15$ μF.

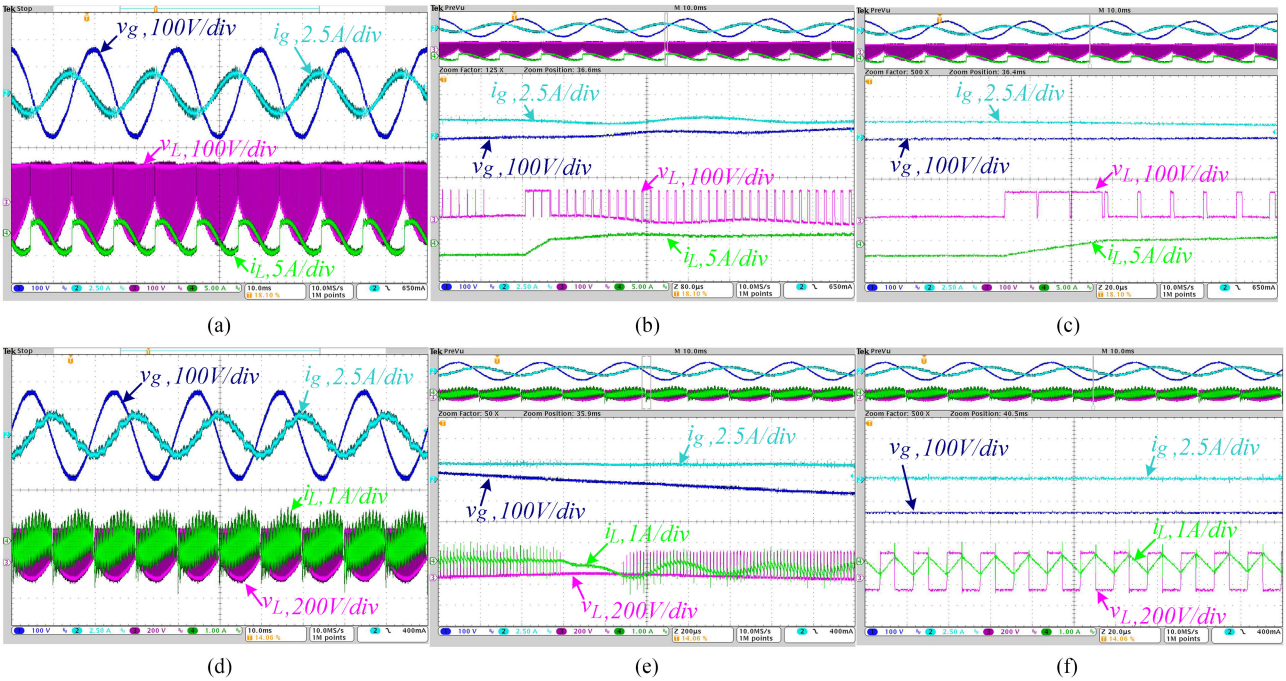

Fig. 11. Experimental results with the generation of reactive power for the twisted buck–boost inverter based on the unfolding circuit: (a) positive shifting on 90° of the grid current, (b) and (c) transient process of the inductor current and voltage at zero crossing with 90° of grid current shifting, (d) shifting on $-90°$ of the grid current, (e) transient process of the inductor current and voltage at zero crossing with $-90°$ of grid current shifting, and (f) high-switching ripples of the inductor current with 30 μF of the unfolding capacitor.

a 30 μF capacitor in the unfolding circuit [see Fig. 12(d)–(f)]. MPC can keep a good THD value of the grid current in this second case as well, even with the current step. However, it required a higher horizon of prediction to get a more stable current in the inductance. Fig. 12(e) and (f) shows the current step from 4 A of the active power to 2 A of the reactive power while the input voltage is 120 V.

Fig. 13 shows different dynamic reference current changes in case the small unfolder capacitor equals 1.3 μF [see Fig. 13(a)–(c)] and the increased unfolder capacitor 30 μF [see Fig. 13(d)–(f)].

One of the advantages of using MPC is the possibility to track very fast the reference current value without a soft-start. However, the relay connection can cause a current spike in the grid side because the turn-on time of the relay cannot be defined exactly. The solution is to pre-charge the unfolding capacitor to the grid voltage, as shown in Fig. 13(a)–(e).

Fig. 13(c) and (f) shows the experimental results of the dynamic response with the twisted buck–boost inverter based on the unfolding circuit. In the first case, the grid current changes from 8 A of the active power to 2 A of the reactive power with a phase shift of 90° to the grid voltage. The experimental results did not show abnormal shapes of the grid current during the current step. MPC allowed us to avoid any spikes during the transient process, going very fast to the new reference current value. The second case corresponds to a negative phase shift of

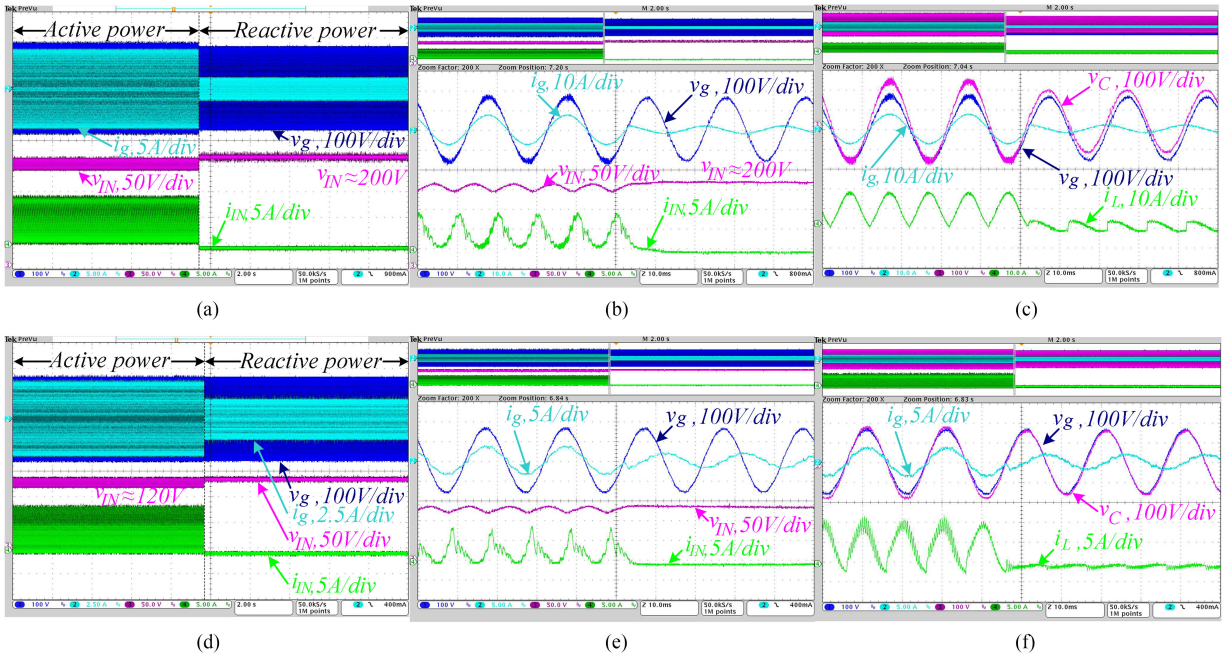

Fig. 12. Experimental results for the dynamic response of the twisted buck–boost inverter based on the unfolding circuit: (a)–(c) positive phase shift 90° of the grid current, and (d)–(f) buck–boost case on the negative phase shift of the grid current with unfolding capactor 30 μF.

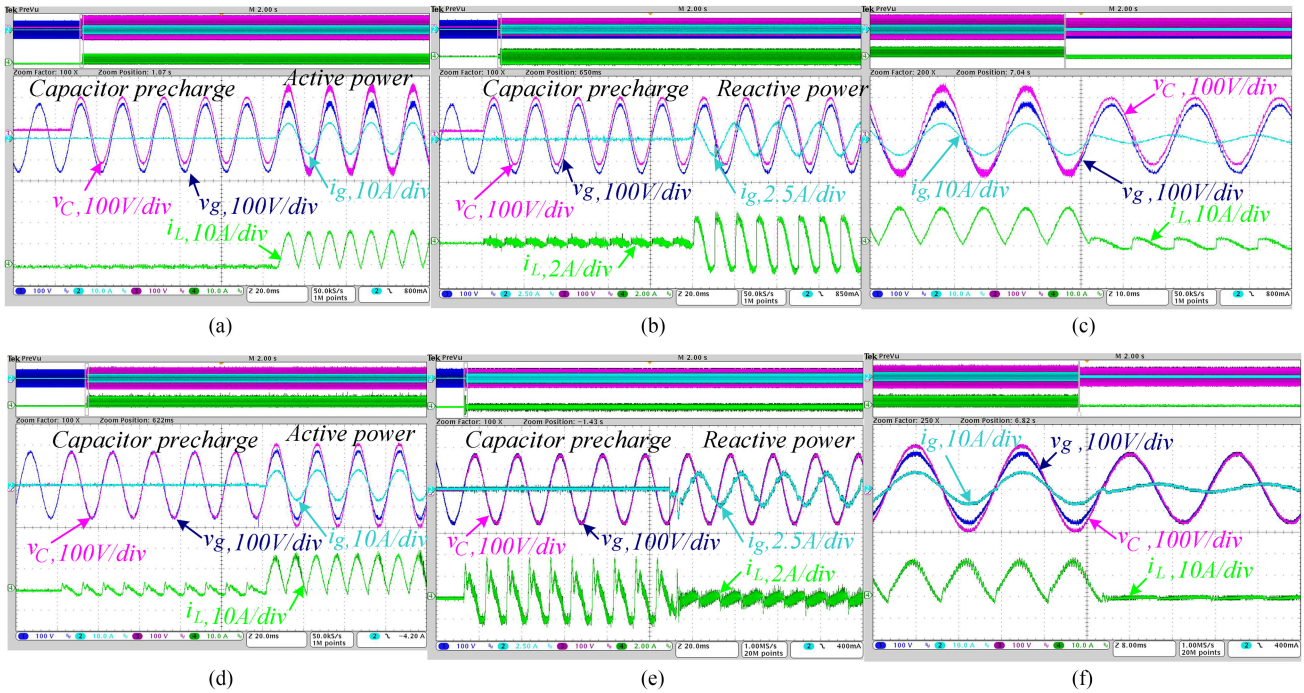

Fig. 13. Experimental results for the twisted buck–boost inverter based on the unfolding circuit: (a) soft-start of the active power generation, (b) soft-start of the reactive power generation with capacitor precharge and positive phase shift, (c) current jump response with the changing mode of the grid reactive power injection, (d) soft-start of the active power generation with the increased capacitor of the unfolding circuit to 30 μF, (e) soft-start of the reactive power injection to the grid with current phase −90°, and (f) current step from active power to reactive with increased capacitor of the unfolding circuit to 30 μF.

−90° of the grid current and the same step (from 8 A of the active power to 2 A of the reactive power,) with a 30 μF capacitor in the unfolding circuit [see Fig. 13(f)]. MPC can keep a good THD value of the grid current in this second case as well, even with the current step.

VI. Conclusion

The recently proposed family based on the single-phase buck–boost inverter with unfolding circuits is a suitable solution for renewable energy applications. To address the power quality

standards, such systems have to contribute to voltage support by delivering reactive power. However, this statement has been questioned in some recent papers [27], [28], since the conventional inverters based on unfolding circuits operate at the unity power factor. Our work has demonstrated how the reactive power can be injected (both pure inductive and pure capacitive reactive power) using these topologies. In the case of the pure inductive reactive power injection, the pure sinusoidal shape of current can be achieved with a very small unfolding capacitor initially calculated for active power generation. In the case of pure capacitive reactive power injection, a good quality grid current waveform can be achieved by an increased value of the unfolding capacitors.

The studied feature makes this solution even more interesting for low voltage grid-connected applications as it can provide ancillary services to the utility.

REFERENCES

[1] D. Meneses, O. García, P. Alou, J. A. Oliver, and J. A. Cobos, "Grid-connected forward microinverter with primary-parallel secondary-series transformer," *IEEE Trans. Power Electron.*, vol. 30, no. 9, pp. 4819–4830, Sep. 2015.

[2] S. Jiang, D. Cao, Y. Li, and F. Z. Peng, "Grid-connected boost-half-bridge photovoltaic microinverter system using repetitive current control and maximum power point tracking," *IEEE Trans. Power Electron.*, vol. 27, no. 11, pp. 4711–4722, Nov. 2012.

[3] R. Carnieletto, D. I. Brandão, F. A. Farret, M. G. Simões, and S. Suryanarayanan, "Smart grid initiative," *IEEE Ind. Appl. Mag.*, vol. 17, no. 5, pp. 27–35, Sep./Oct. 2011.

[4] Y. Yang, F. Blaabjerg, H. Wang, and M. G. Simões, "Power control flexibilities for grid-connected multi-functional photovoltaic inverters," *IET Renewable Power Gener.*, vol. 10, no. 4, pp. 504–513, 2016.

[5] P. Sun, C. Liu, J. Lai, C. Chen, and N. Kees, "Three-phase dual-buck inverter with unified pulsewidth modulation," *IEEE Trans. Power Electron.*, vol. 27, no. 3, pp. 1159–1167, Mar. 2012.

[6] Z. Yao and L. Xiao, "Two-switch dual-buck grid-connected inverter with hysteresis current control," *IEEE Trans. Power Electron.*, vol. 27, no. 7, pp. 3310–3318, Jul. 2012.

[7] R. O. Caceres and I. Barbi, "A boost DC-AC converter: Analysis, design, and experimentation," *IEEE Trans. Power Electron.*, vol. 14, no. 1, pp. 134–141, Jan. 1999.

[8] F. Gao, R. Teodorescu, F. Blaabjerg, P. C. Loh, and D. M. Vilathgamuwa, "Performance evaluation of buck-boost three-level inverters with topological and modulation development," in *Proc. Eur. Conf. Power Electron. Appl.*, 2007, pp. 1–10.

[9] F. Gao, P. C. Loh, R. Teodorescu, F. Blaabjerg, and D. M. Vilathgamuwa, "Topological design and modulation strategy for buck–boost three-level inverters," *IEEE Trans. Power Electron.*, vol. 24, no. 7, pp. 1722–1732, Jul. 2009.

[10] Y. Liu, H. Abu-Rub, and B. Ge, "Z-source\/quasi-Z-source inverters: Derived networks, modulations, controls, and emerging applications to photovoltaic conversion," *IEEE Ind. Electron. Mag.*, vol. 8, no. 4, pp. 32–44, Dec. 2014.

[11] O. Husev *et al.*, "Comparison of impedance-source networks for two and multilevel buck–boost inverter applications," *IEEE Trans. Power Electron.*, vol. 31, no. 11, pp. 7564–7579, Nov. 2016.

[12] V. Jagan, J. Kotturu, and S. Das, "Enhanced-Boost quasi-Z-source inverters with two-switched impedance networks," *IEEE Trans. Ind. Electron.*, vol. 64, no. 9, pp. 6885–6897, Sep. 2017.

[13] D. Panfilov, O. Husev, F. Blaabjerg, J. Zakis, and K. Khandakji, "Comparison of three-phase three-level voltage source inverter with intermediate dc-dc boost converter and quasi-Z-source inverter," *IET Power Electron.*, vol. 9, no. 6, pp. 1238–1248, 2016.

[14] D. C. Martins and R. Demonti, "Grid connected PV system using two energy processing stages," in *Proc. Conf. Rec. 29th IEEE Photovolt. Specialists Conf.*, 2002, pp. 1649–1652.

[15] P. Wolfs and Q. Li, "An analysis of a resonant half bridge dual converter operating in continuous and discontinuous modes," in *Proc. IEEE 33rd Annu. IEEE Power Electron. Specialists Conf* ., 2002, vol. 3, pp. 1313–1318.

[16] D. C. Martins and R. Demonti, "Interconnection of a photovoltaic panels array to a single-phase utility line from a static conversion system," in *Proc. 31st Annu. Power Electron. Specialists Conf.*, 2000, vol. 3, pp. 1207–1211.

[17] E. Achille, T. Martire, C. Glaize, and C. Joubert, "Optimized DC-AC boost converters for modular photovoltaic grid-connected generators," in *Proc. IEEE Int. Symp. Ind. Electron.*, 2004, vol. 2, pp. 1005–1010.

[18] K. C. A. de Souza, M. R. de Castro, and F. Antunes, "A DC/AC converter for single-phase grid-connected photovoltaic systems," in *Proc. IEEE 28th Annu. Conf. Ind. Electron. Soc.*, 2002, vol. 4, pp. 3268–3273.

[19] H. Fujimoto, K. Kuroki, T. Kagotani, and H. Kidoguchi, "Photovoltaic inverter with a novel cycloconverter for interconnection to a utility line," in *Proc. IEEE Ind. Appl. Conf. 30th IAS Annu. Meeting*, 1995, vol. 3, pp. 2461–2467.

[20] D. Li, C. N. M. Ho, L. Liu, and G. Escobar, "Reactive power control for single-phase grid-tie inverters using quasi-sinusoidal waveform," *IEEE Trans. Sustain. Energy*, vol. 9, no. 1, pp. 3–11, Jan. 2018.

[21] D. Neumayr, D. Bortis, and J. W. Kolar, "The essence of the little box challenge-part A: Key design challenges & solutions," *CPSS Trans. Power Electron. Appl.*, vol. 5, no. 2, pp. 158–179, Jun. 2020.

[22] D. Neumayr, D. Bortis, and J. W. Kolar, "The essence of the little box challenge-part B: Hardware demonstrators & comparative evaluations," *CPSS Trans. Power Electron. Appl.*, vol. 5, no. 3, pp. 251–272, Sep. 2020.

[23] E. Fonkwe, J. Kirtley, and J. Elizondo, "Flyback micro-inverter with reactive power support capability," in *Proc. IEEE 17th Workshop Control Model. Power Electron.*, 2016, pp. 1–8.

[24] O. Husev, O. Matiushkin, C. Roncero-Clemente, F. Blaabjerg, and D. Vinnikov, "Novel family of single-stage buck-boost inverters based on unfolding circuit," *IEEE Trans. Power Electron.*, vol. 34, no. 8, pp. 7662–7676, Aug. 2019.

[25] O. Matiushkin, O. Husev, D. Vinnikov, and C. Roncero-Clemente, "Optimal LCL-filter study for buck-boost inverter based on unfolding circuit," in *Proc. IEEE 14th Int. Conf. Compat., Power Electron. Power Eng.*, 2020, pp. 1–6.

[26] O. Husev, O. Matiushkin, D. Vinnikov, C. Roncero, E. Romero-Cadaval, and L. Kutt, "Buck-boost unfolder inverter as a novel solution for single-phase PV systems," in *Proc. 44th Annu. Conf. IEEE Ind. Electron. Soc.*, 2018, pp. 6116–6121.

[27] U. A. Khan and J. -W. Park, "Full-bridge single-inductor-based buck–boost inverters," *IEEE Trans. Power Electron.*, vol. 36, no. 2, pp. 1909–1920, Feb. 2021.

[28] A. A. Khan, Y. W. Lu, U. A. Khan, L. Wang, W. Eberle, and M. Agamy, "Novel transformerless buck–boost inverters without leakage current," *IEEE Trans. Ind. Electron.*, vol. 67, no. 12, pp. 10442–10454, Dec. 2020.

[29] W. Li, Y. Gu, W. Cui, X. He, and C. Xia, "Topology review and derivation methodology of single-phase transformerless photovoltaic inverters for leakage current suppression," *IEEE Trans. Ind. Electron.*, vol. 62, no. 7, pp. 4537–4551, Jul. 2015.

[30] O. Matiushkin, O. Husev, J. Rodriguez, H. Young, and I. Roasto, "Feasibility study of model predictive control for grid-connected twisted buck-boost inverter," *IEEE Trans. Ind. Electron.*, vol. 69, no. 3, pp. 2488–2499, Mar. 2022.

[31] Q. Li and P. Wolfs, "A review of the single phase photovoltaic module integrated converter topologies with three different DC link configurations," *IEEE Trans. Power Electron.*, vol. 23, no. 3, pp. 1320–1333, May 2008.

[32] O. Matiushkin, O. Husev, R. Strzelecki, S. Ivanets, and A. Fesenko, "Novel single-stage buck-boost inverter with unfolding circuit," in *Proc. IEEE 1st Ukraine Conf. Elect. Comput. Eng.*, 2017, pp. 538–543, doi: 10.1109/UKRCON.2017.8100298.

[33] S. F. Zarei, H. Mokhtari, M. A. Ghasemi, S. Peyghami, P. Davari, and F. Blaabjerg, "DC-link loop bandwidth selection strategy for grid-connected inverters considering power quality requirements," *Int. J. Elect. Power Energy Syst.*, vol. 119, 2020, Art. no. 105879, doi: 10.1016/j.ijepes.2020.105879.

[34] O. Matiushkin, O. Husev, C. Roncero-Clemente, S. Ivanets, and A. Fesenko, "Component design guidelines for new single-stage buck-boost inverter with unfolding circuit," in *Proc. IEEE Int. Young Sci . Forum Appl. Phys. Eng.*, 2017, pp. 40–45, doi: 10.1109/YSF.2017.8126589.

[35] H. Hu, S. Harb, N. Kutkut, I. Batarseh, and Z. Shen, "A review of power decoupling techniques for micro-inverters with three different decoupling capacitor locations in PV systems," *IEEE Trans. Power Electron.*, vol. 28, no. 6, pp. 2711–2726, Jun. 2012.

[36] Y. Sun, Y. Liu, M. Su, W. Xiong, and J. Yang, "Review of active power decoupling topologies in single-phase systems," *IEEE Trans. Power Electron.*, vol. 31, no. 7, pp. 4778–4794, Jul. 2016.

Carlos Roncero-Clemente (Member, IEEE) received the international Ph.D. degree in electrical, electronic, and control engineering from the University of Extremadura, Badajoz, Spain, in 2016.

During his Ph.D. research, he was a visiting student with the Tallinn University of Technology and Aalborg University. He was a postdoctoral researcher with the Nova University of Lisbon (2016–2019). He is currently a senior researcher in power electronic and renewable energies with the University of Extremadura. He is an author of more than 30 journal papers and 75 international conferences. His research interests include power electronic topologies and controls for renewable energy applications and smart grids.

Oleksandr Husev (Senior Member, IEEE) received the B.Sc. and M.Sc. degrees in industrial electronics from Chernihiv State Technological University, Chernihiv, Ukraine, in 2007 and 2008, respectively, and the Ph.D. degree from the Institute of Electrodynamics of the National Academy of Science of Ukraine, Kyiv, Ukraine, in 2012.

He is currently a senior researcher and a project leader with the Department of Electrical Power Engineering and Mechatronics, TalTech University, Tallinn, Estonia. He is an author of more than 100 publications and is the holder of several patents. His research interests include power electronics systems, design of novel topologies, control systems based on a wide range of algorithms, including modeling, design, and simulation, applied design of power converters and control systems and applications, and stability investigation.

Oleksandr Matiushkin (Student Member, IEEE) received the B.Sc. and M.Sc. degrees in industrial electronics from the Chernihiv National University of Technology, Chernihiv, Ukraine, in 2016 and 2018, respectively. He is currently working toward the Ph.D. degrees (double doctoral study) with the Tallinn University of Technology, Tallinn, Estonia, and the Chernihiv National University of Technology, working on power electronics.

He was a Junior Researcher with the Department of Electrical Engineering, Tallinn University of Technology. His research interests include modeling, calculation of dynamic processes, design and control converters for photovoltaic applications, and applied design of new topologies of power electronics converters.

Dmitri Vinnikov (Senior Member, IEEE) received the Dipl.Eng., M.Sc., and Dr.Sc.techn. degrees in electrical engineering from Tallinn University of Technology, Tallinn, Estonia, in 1999, 2001, and 2005, respectively.

He is currently the Head of the Power Electronics Group, Department of Electrical Power Engineering and Mechatronics, Tallinn University of Technology. He is the Head of R&D and cofounder of Ubik Solutions LLC—an Estonian start-up company dedicated to innovative and smart power electronics for renewable energy systems. Moreover, he is one of the founders and leading researchers of ZEBE – Estonian Centre of Excellence for zero energy and resource efficient smart buildings and districts. He has authored or coauthored 2 books and 5 monographs as well as more than 400 published papers on power converter design and development and is the holder of numerous patents and utility models in this field. His research interests include applied design of power electronic converters and control systems, renewable energy conversion systems (photovoltaic and wind), and implementation of wide bandgap power semiconductors.

D. Vinnikov is the Chair of the IEEE Estonia Section.

Frede Blaabjerg (Fellow, IEEE) received the Ph.D. degree in electrical engineering from Aalborg University, Aalborg, Denmark, in 1995.

From 1987 to 1988, he was with ABB-Scandia, Randers, Denmark. He became an Assistant Professor in 1992, an Associate Professor in 1996, and a Full Professor of power electronics and drives in 1998 at AAU Energy, Aalborg, Denmark. In 2017, he became a Villum Investigator. He was an author of more than 600 journal papers in the fields of power electronics and its applications. He is a coauthor of four monographs and an editor of ten books in power electronics and its applications. His current research interests include power electronics and its applications such as in wind turbines, PV systems, reliability, harmonics, and adjustable speed drives.

Dr. Blaabjerg was the Editor-in-Chief for the IEEE TRANSACTIONS ON POWER ELECTRONICS from 2006 to 2012. He has been a Distinguished Lecturer for the IEEE Power Electronics Society from 2005 to 2007 and for the IEEE Industry Applications Society from 2010 to 2011 as well as 2017 to 2018. During 2019–2020, he was the President of IEEE Power Electronics Society. He has been the Vice-President of the Danish Academy of Technical Sciences. He is nominated during 2014–2020 by Thomson Reuters to be among the most 250 cited researchers in engineering in the world. He was the recipient of 33 IEEE Prize Paper Awards, the IEEE PELS Distinguished Service Award in 2009, the EPE-PEMC Council Award in 2010, the IEEE William E. Newell Power Electronics Award 2014, the Villum Kann Rasmussen Research Award 2014, the Global Energy Prize in 2019 and the 2020 IEEE Edison Medal.